16th World Conference on Earthquake, 16WCEE 2017
Santiago Chile, January 9th to 13th 2017
Paper N° 847 (Abstract ID)
Registration Code: S-K1461808524

Experimental and numerical analysis on seismic behavior of composite concrete and double steel plates shear wall with binding bars

Chunlan. Cheng[(1)], Deyuan. Zhou[(2)]

[(1)] *Lecturer, Institute of Structural Engineering and Disaster Reduction, Tongji University, China. cclan83@126.com*

[(2)] *Professor, Institute of Structural Engineering and Disaster Reduction, Tongji University, China. dyzhou@tongji.edu.cn*

Abstract

With the increase of building height and the advance function requirement of architecture, the higher performance demand of structural walls were proposed. Steel plate -concrete composite walls with binding bars are one of the new-style structural walls and have already been employed in the actual practice in recent years. The composite walls comprise of steel plates connected by an array of transverse binding bars using bolt connections and filled with concrete. In order to intensively investigate the seismic behavior of this new type of concrete filled double-steel-plate composite wall, The experimental and numerical analysis on seismic behavior of composite concrete and double steel plates shear wall with binding bars (CCSPW) subject to cyclic loading are discussed in this paper. Firstly, sixteen specimens are tested under large axial compressive force and reversed cyclic lateral load. The failure modes and deformation performance were observed. Valuable results were obtained for the hysteretic loops, shearing capacity, skeleton curves, ductility and other parameters. The surface steel and infill concrete can work compatibly by the binding bar connections in the whole process. All the specimens exhibited good energy dissipation ability and deformation capacity with full hysteretic curves and large ultimate drift ratios. Secondly, nonlinear finite element models were built with analytical software OpenSees. The simulations of hysteresis curves are conducted and the results agreed well with the test results. On the basis of that, parameter analyses of the CCSPW were carried out. Thirdly, the empirical formula to computing lateral shearing capacity and deformation of the composite shear walls with binding bars were derived by numerical fitting. And furthermore the hysteresis loop of the specimens under hysteretic load was confirmed by quantitative computation. The calculated value coincides well with the experimental value. All the experimental and numerical results indicate that the seismic performance of composite concrete and steel plate shear walls with binding bars is good and the seismic performance is enhanced with different factors. Some valuable results can give reference to the design and research of the new style shear walls.

Keywords: binding bars, cyclic loading test, parameter analyses, skeleton curve, hysteresis loop

1. Introduction

The shear walls are one of the most critical elements in the high-rise or super high-rise structural system, which have long been used as an efficient lateral force-resisting system for building. With the increase of building height and the advance function requirement of architecture, the higher performance demand of structural walls were proposed. Steel plate -concrete composite walls are one of the new-style structural walls and have already been employed in the actual practice in recent years. It can be classified as steel plate reinforced concrete composite walls (SPRC) and concrete filled double steel plate (CFDSP) composite walls according to the different relative positions of the steel plates and concrete. Base on the interaction and cooperation of the two materials, the mechanical behavior of shear walls prominently changes.

Many researchers have carried out experimental and analytical studies on CFDSP walls in the past years, and several different configurations have been proposed. It was applied in the nuclear facilities, marine environment structures because of its superior behavior, large lateral stiffness, low cost and rapid construction. Wright et al. [1] conducted some pilot studies on the composite wall formed from two skins of profiled steel sheeting filled with concrete under different loading conditions and found that the steel sheeting provides similar characteristics to conventional framework for concrete casting and finally to establish design formulas for actual practice [2–6] (Fig. 1a). Three 1/4 scale specimens of CFDSP walls with both horizontal and vertical diaphragms were built to take cyclic shear loading test by Emori K. [7] (Fig. 1b). The shear test exhibited high strength and significant ductility of these kinds of walls. Welded connection was used between the insert plates and the long-side steel plate, which would result in the deficiency of the steel plates and be difficult to be applied to the engineering. The Corus Company developed a CFDSP construction called Bi-Steel™ [8] with two surface steel plates connected by an array of transverse friction welded shear connectors (Fig. 1c), and a series of researches have been conducted on Bi-Steel [9–11].

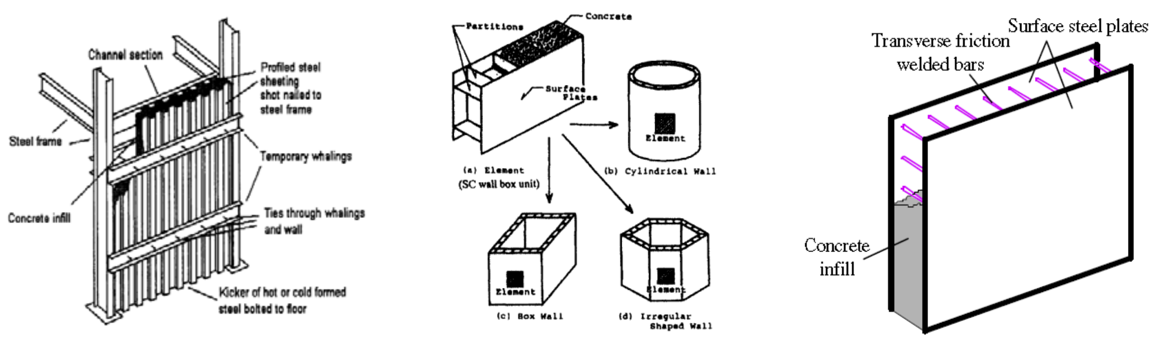

(a) Proposed by Wright [1] (b) Proposed by Emori [7] (c) Bi-Steel [8]

Fig. 1-Previous developed CFDSP walls

Considering the fact that the elements are hard to fabricate and may bring the residual stress in the steel plate when a large number of weld stud or panel is adopt, the composite concrete and steel plate shear walls with binding bars were proposed. In spite of extensive studies of CFDSP walls in the literature, the CFDSP walls with binding bars have not been fully addressed. In order to intensively investigate the seismic behavior of this new detailed concrete filled double-steel-plate composite wall, the experimental and numerical analysis on seismic behavior of composite concrete and double steel plates shear wall with binding bars (CCSPW) subject to cyclic loading is discussed in this paper. Sixteen wall specimens were tested under axial compressive forces and reversed cyclic lateral loads. Failure mechanism, hysteric behavior, strength and deformation capacities, etc. are discussed in detail. The nonlinear finite element models were built with analytical software OpenSees. Parameter analyses of the CCSPW were carried out. And furthermore the triple line skeleton curve and hysteresis loop of the specimens under hysteretic load was proposed. The feasibility of the configuration was tested, and the features of seismic performance of shear walls were investigated.

2. Experimental Research

2.1 Experimental program

2.1.1 Test Specimens

Sixteen specimens with different parameters were designed and tested under high axial compressive forces and reversed cyclic lateral loads. The cross section and detailing of specimens are illustrated in Fig. 2. Two ends of the specimens were embedded into the reinforced concrete basement and loading beam to simulate the boundary conditions of shear walls in buildings. The main parameters were the aspect ratio, thickness of concrete wall, thickness of long-side steel plate, binding bar spacing, embedded section steel and axial compression ratio. The detail parameters of each specimen are shown in Table 1.The short-side steel plates of all the specimens are C section steel plates with thickness of 6mm.

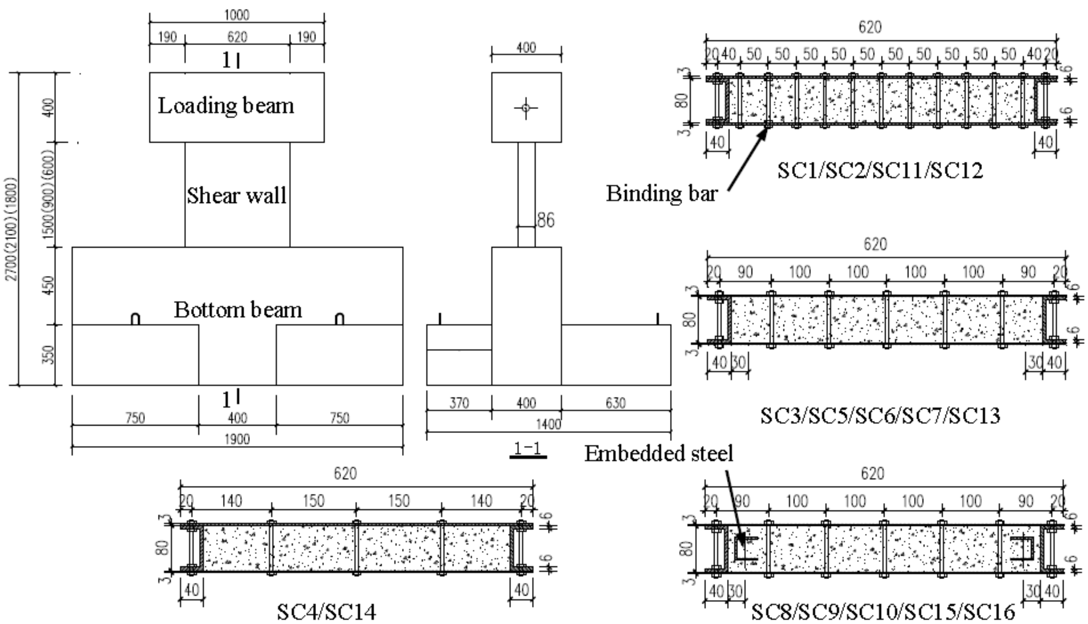

(a) Cross section

(b) Specimen construction (c) Bolt connection with eight nuts (d) Specimen installation

Fig. 2— Deta iling of Specimens of Composite concrete-steel plate shear walls with binding bars

Table 1—Tested specimens

Specimen	Dimension of cross section(mm) (width×depth)	Aspect ratio	Long-side plate thickness(mm)	Binding bar spacing (mm)	Embedded section steel	Axial compression ratio (*n*)
SC1	620×86	1.5	3.0	50	No	0.4
SC 2	620×86	1.5	3.0	50	No	0.3
SC 3	620×86	1.5	3.0	100	No	0.3
SC 4	620×86	1.5	3.0	150	No	0.3
SC 5	620×86	2.5	3.0	100	No	0.3
SC 6	620×88	2.5	4.0	100	No	0.3
SC 7	620×106	2.5	3.0	100	No	0.3
SC 8	620×86	2.5	3.0	100	C40×40×4	0.3
SC 9	620×86	1.5	3.0	100	C40×40×4	0.3
SC 10	620×86	1.5	3.0	100	C40×40×4	0.4
SC 11	620×86	1.0	3.0	50	No	0.4
SC 12	620×86	1.0	3.0	50	No	0.4
SC 13	620×86	1.0	3.0	100	No	0.3
SC 14	620×86	1.0	3.0	150	No	0.3
SC 15	620×86	1.0	3.0	100	C40×40×4	0.3
SC 16	620×86	1.0	3.0	100	C40×40×4	0.3

2.1.2 Materials

All the walls were constructed with steel plates, binding bars and concrete. The average compressive strength (f_{cu}) of concrete was obtained by the test of nine cube samples (150×150×150mm), which gives f_{cu} =31.58MPa with a standard deviation of 1.19MPa. The yield stress of steel plates with 3mm thickness is 321.7 N/mm^2. The ultimate stress of steel plates with 3mm thickness is 465.6 N/mm^2.

2.1.3 Test setup and loading procedure

The test setup is shown in Fig.3. The axial compressive force N was first applied to the specimen by three vertical hydraulic jacks, which was maintained constant by a pressure gauge. N was calculated from Eq. (1)

when n was given in Table 1. fc is the compressive strength of concrete; fy is the yield strength of steel plates; Ac and As are the cross-sectional areas of concrete and steel plates, respectively.

$$N=n\,(f_{ck}\,A_c+f_{yk}\,As) \tag{1}$$

The lateral force was first controlled by load and then by top displacement. In the load control stage, the initial lateral load is set as 25 percent of the estimated yielding force. Before coming to the estimated yielding force, the applied load increases by a 20kN interval gradually at the beginning and a 10kN interval when close to the estimated yielding force. After exceeding the estimated yielding force, the loading scheme changes to a displacement controlled mode. Each loading step includes one complete cycle in the force-controlled phase and three cycles in the displacement-controlled phase. When the lateral force dropped below 85% of the maximum strength or the axial force could not be sustained, the test was stopped.

2.1.4 Instrumentation

All the specimens were instrumented to measure the loads, displacements and strains at critical locations. The arrangement of displacement meter is shown in Fig.4. The top displacement meters (DT 1) which at the same height of the loading point is used to measure the main value of the lateral displacements. Steel strain gauges were arranged at different locations to measure the strain distribution of the specimens. Binding bars were chosen of each specimen to measure their stressing state.

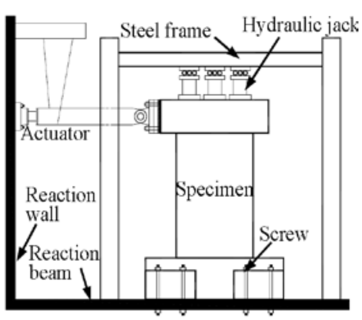

Fig. 3— Test setup

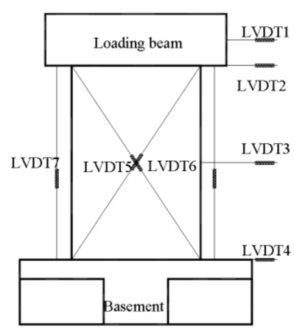

Fig. 4— Measuring points arrangement

2.2 Experimental results

2.2.1. Failure modes

The macroscopic damage occurred at the base of the wall in all specimens. Obvious local buckling, plastic deformation, out-plane instability, fracture and the crack of the concrete were observed. For all specimens, the local buckling took place in the bolt connection area of the long-side steel plate at margin of the bottom, some specimens even developed fracture. It found that the corner area of the core concrete crushed and the vertical cracks or diagonal cracks appeared in the wall by removing steel plate after the test.

Take specimen SC5, SC4, SC14 as the example, the failure mode is shown in Fig. 5. The loading process could be divided into three stages: pre-yielding stage (from beginning to yielding point on the load-displacement envelope curve), plastic stage (from yielding point to the peak point) and failure stage. The skeleton loops are shown in Fig. 6.

(a)SC5 (b)SC4 (c)SC14

Fig. 5— Failure process and modes

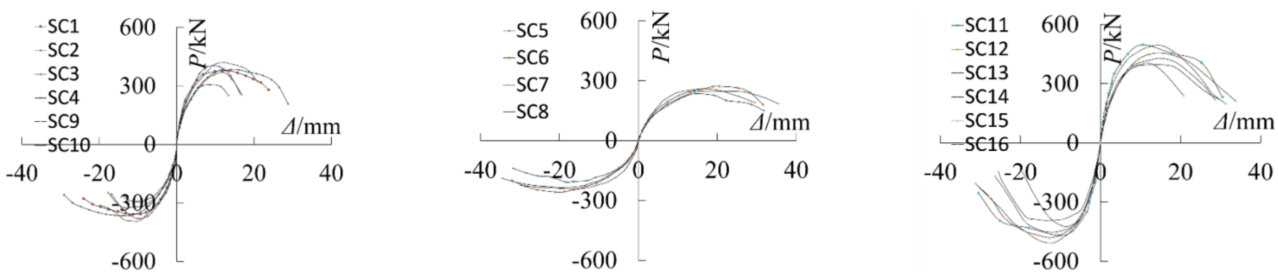

(a)Specimen with aspect ratio 1.5 (b) Specimen with aspect ratio 2.5 (c) Specimen with aspect ratio 1.0

Fig. 6—Lateral force-displacement skeleton loops

2.2.2 Shearing capacity and deformation

The test results for all specimens are illustrated in Table 2. As we can see from the data, increases of the thickness of steel plate or concrete, embedment of channel steel, decreasing the spacing of binding bars can improve the shearing capacity of specimen. Increase the axial compression ration can reduce the shearing capacity when the value of n is high.

Table 2—The typical values of lateral force and displacement

NO.	Yielding state		Peak state		Failure state		Ductility
	P_y(kN)	Δ_y(mm)	P_u(kN)	Δ_u/mm	P_d(kN)	Δ_d/mm	$\mu=\Delta_d/\Delta_y$
SC1	311.6	4.93	368.4	12.51	313.3	21.69	4.404
SC2	313.1	6.80	374.0	15.05	317.5	25.63	3.768
SC3	289.4	5.92	348.9	12.20	296.5	15.84	2.675
SC4	246.1	4.53	299.5	9.35	263.4	13.39	2.956
SC5	184.6	8.96	221.7	16.45	188.4	24.58	2.744
SC6	220.5	10.90	264.7	20.80	225.0	29.09	2.669
SC7	198.5	9.52	241.8	19.45	205.5	32.75	3.442
SC8	214.1	7.84	251.5	16.30	222.5	27.71	3.534
SC9	337.1	6.10	406.6	11.60	345.6	18.24	2.992

SC10	315.7	4.85	392.6	9.85	333.7	14.28	2.946
SC11	377.1	4.36	482.8	10.57	410.4	23.58	5.407
SC12	376.4	6.03	467.8	14.06	397.6	22.85	3.790
SC13	351.2	5.40	441.0	13.54	374.8	20.47	3.787
SC14	337.1	4.59	409.6	11.23	348.2	15.01	3.270
SC15	388.7	5.45	499.7	13.52	424.7	20.39	3.739
SC16	326.8	5.04	394.2	12.75	335.0	20.82	4.130

3. Numerical analysis

3.1 Numerical Modeling

The numerical simulation by using the analytical software OpenSees was conducted on the CCSPW with binding bars. The numerical model shows in Figure 7. The outer steel plate and the inner concrete wall were simulated as cohesive joint without considering the bond-slip between them. The edge members were simulated using Displacement Based Beam-Column Element. The concrete and the profile steel were modeled using Concrete02 and Steel02 constitutive relation, respectively. Quad Element was applied to simulate the concrete shear wall plate and the outside steel plate. J2 Plasticity Material model was used to define the material in the simulation.

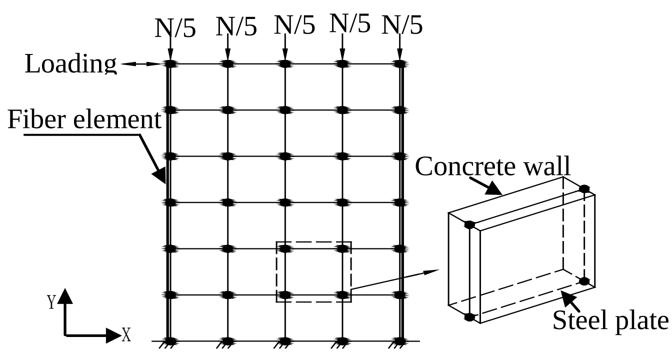

Fig. 7—OpenSees numerical model

The calculated value coincides well with the experimental value by comparison. It indicates that the numerical simulation can objectively reflect the loading process of this kind of shear walls. The comparison charts of the typical specimens are shown in Fig. 8

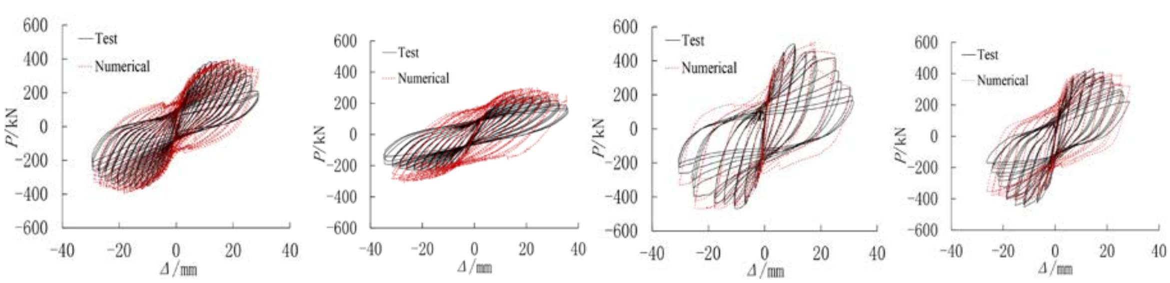

(a) SC2 (b) SC7 (c) SC11 (d) SC13

Fig. 8—Lateral force-displacement hysteretic loops

3.2 Parameter analyses

All the results indicate that the factors of aspect ratios, axial compression ratios and binding bar spacing dramatically affected the seismic performance of this kind of shear walls. The relationships of lateral force versus different parameters are shown in Fig. 9.

The change tendency of the shearing capacity of the component with the aspect ratio is shown in Fig 9(a). With the increase of the aspect ratios of the composite concrete and steel plate shear walls, the shearing capacity decreased obviously. Its trend line can adopt the function of the index to fit. The change tendency of the shearing capacity of the component with the axial compression ratio is shown in Fig 9(b). The change of axial compression ratio has a certain effect on the horizontal shearing capacity of composite shear walls, but the influence is limited. The trend line is basically linear. The change tendency of the shearing capacity of the component with the binding bar spacing is shown in Fig 9(c). In addition, the decrease of binding bars spacing can improve the shearing capacity. The trend line is basically linear.

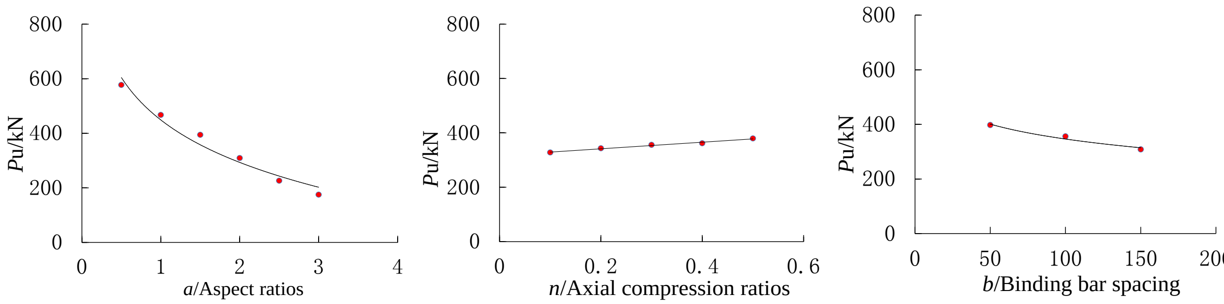

(a) Aspect ratio (b) Axial compression ratios (c)Binding bar spacing

Fig. 9—Relationship on lateral force- different parameters

4 Lateral shearing capacity and deformation

After making parametric analysis and using the method of shearing capacity superposition, the empirical formula to computing lateral shearing capacity and deformation of the composite shear walls with binding bars were derived by numerical fitting.

4.1 Shearing capacity and the corresponding displacement

Based on the formula of shearing capacity [12], and considering the influence of the aspect ratio, the axial compression ratio and the binding bar spacing, the formula was fitted with the test value of the maximum shearing capacity. The fitting coefficient law refers to the trend line of each parameter proposed in the previous section.

$$P_u = \left(\frac{0.75}{1+1.35a} + 0.3e^{-0.6a} \right) \left[0.15 f_{\mathrm{ck}} b_{\mathrm{c}} L_{\mathrm{c}} (1+5\zeta) + 0.15N + 0.6 f_{\mathrm{y}} A_{\mathrm{s}} \right] \tag{2}$$

$$\zeta = \frac{A_{\mathrm{b}} f_{\mathrm{by}}}{b b_{\mathrm{c}} f_{\mathrm{ck}}} \tag{3}$$

The displacement corresponding the peak load can be calculated from Eq. (4)

$$\Delta_{\mathrm{u}} = \frac{(1.7+n+10\zeta) P_{\mathrm{u}}}{K_{\mathrm{a}}} \tag{4}$$

Where ζ is the effect coefficient that considering the constraint of outer steel plate on core concrete; b is the binding bar spacing; A_b is the sectional area of binding bar; a is aspect ratio of shear wall; f_{ck} is the axial compressive strength of concrete; b_c is the width of core concrete section，L_c is the height of core concrete section；N is the axial load；f_y is the yield strength of steel plate and end section steel; A_s is the sectional area of steel plate and end section steel on one side; n is the axial compression ratio

The calculated value coincides well with the experimental value. The comparison between calculated and experimental values of shearing capacity and peak displacement are shown in table 3.

Table 3— comparison in bearing capicity of calculated value and experimental value

NO	Experimental value $P_{t,u}$/kN	Calculated value $P_{c,u}$/kN	$P_{c,u}/P_{t,u}$	Experimental value $\Delta_{t,u}$/mm	Calculated value $\Delta_{c,u}$/mm	$\Delta_{c,u}/\Delta_{t,u}$
SC1	368.4	383.7	1.042	12.51	15.10	1.21
SC2	374.0	374.0	1.000	15.05	14.31	0.95
SC3	348.9	348.0	0.998	12.20	10.48	0.86
SC4	299.5	339.4	1.133	9.35	9.30	0.99
SC5	221.7	224.3	1.012	16.45	18.62	1.13
SC6	264.7	251.0	0.948	20.80	16.77	0.81
SC7	241.8	241.3	0.998	19.45	17.87	0.92
SC8	251.5	244.8	0.973	16.30	16.36	1.00
SC9	406.6	379.8	0.934	11.60	9.21	0.79
SC10	392.6	389.5	0.992	9.85	9.79	0.99
SC11	482.8	501.8	1.039	10.57	14.37	1.36
SC12	467.8	489.2	1.046	14.06	13.62	0.97
SC13	441.0	455.2	1.032	13.54	9.98	0.74
SC14	409.6	443.8	1.084	11.23	8.85	0.79
SC15	499.7	496.8	0.994	13.52	9.08	0.67
SC16	394.2	509.4	1.292	12.75	9.65	0.76

4.2 Yield load and Damage load

From the test and numerical results, we can see the composite shear wall members have no definite yield point under the horizontal force. When the horizontal load reached to approximately 60% of the peak load, the hysteretic skeleton curve occurred a distinctive turning point. Accordingly, The yield load is defined as 60% of peak load, which is shown in Eq.(5)

$$P_y = 0.6P_u \tag{5}$$

The damage load of composite wall is defined as the point which value fell to 85% of peak load. It can be shown in Eq.(6)

$$P_d = 0.85P_u \tag{6}$$

4.3 The initial stiffness

The initial stiffness is only related to the geometric parameters of the component, which can be calculated using Eq.(7)

$$K_e = E_s I_s + 0.2 E_c I_c \tag{7}$$

The initial lateral stiffness of the composite shear wall can be expressed as Eq.(8)

$$K_a = \frac{3K_e}{h^3} \tag{8}$$

Where E_s is the elastic modulus of steel; E_c is the elastic modulus of concrete; I_s is the inertia moment of steel in horizontal plane; I_c is the inertia moment of concrete in horizontal plane; h is the height of the composite shear wall.

Before the component yield, the relationship between carrying capacity and displacement is linear. The yield deformation can be calculated from the initial stiffness and yield load using Eq (9).

$$\Delta_y = \frac{P_y}{K_a} \tag{9}$$

4.4 Degenerated stiffness

The stiffness on the stage of shearing capacity decrease can be obtained by the test data fitting, which can be calculated using Eq.(10)

$$K_t = \frac{-9.83 n^{1.2} a^{0.75} f_y}{E_s \zeta} K_a \tag{10}$$

5. Skeleton curve and Hysteresis loop

From the Eq.(2) to Eq. (10), the key points of the skeleton curve of the shear walls can be calculated quantitatively. The calculated triple line skeleton curve of the specimens under hysteretic load was shown in Fig.10.

Combining the skeleton curve, the hysteretic model of the shear walls under the lateral reciprocating loading was obtained by establishing the components' unloading rigidity and the hysteretic yielding line in the process of unloading.

From the feature of the experimental hysteretic model, the strength degradation is not remarkable under the same displacement corresponding load. And thus it didn't take the strength degradation into account when constructing the hysteretic rules.

Before the yield load, the unloading stiffness of hysteresis loops is equal to the initial stiffness K_a. When the load exceeds the yield load, the unloading stiffness reduces to approximately 80% of the initial stiffness. Consequently it is assumed that the unloading stiffness is equal to 80% of the initial stiffness when the load exceeds the yield load.

The definition of hysteretic yielding is an important part of the hysteretic rules, which reflects the components' state transition from elastic to plastic during the unload stage. When the shear wall is loaded at the elastic stage, the unloading path is returned by the original path. When the load exceeds the yield load，the unloading path goes along the unloading stiffness which defined as 80% of the initial stiffness. In addition, when the unloading load value reaches to about 0.3 times of the initial unloading point, the unloading path goes into the "unloading plastic" stage. At this stage the unloading path points to the reverse load point on the skeleton curve corresponding to the forward unloading point. The defined hysteresis loop of the specimen is shown in Fig.11.

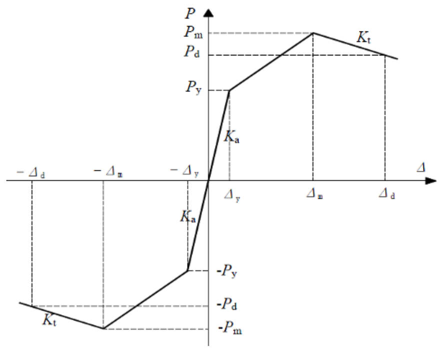

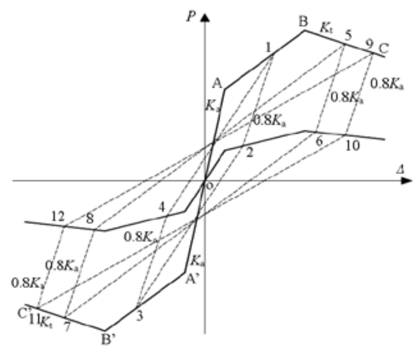

Fig. 10— calculation of skeleton curve　　　　Fig. 11—Hysteresis loop

It demonstrates that the proposed hysteretic model can simulate the shear walls’ hysteretic feature by making a comparison between the hysteretic model and the experimental value of hysteretic curve. The square of the hysteretic model is the same as that of experimental hysteresis loops in the same displacement level, and their envelope curve is similar as well. The comparison in hysteresis loop of calculated value and experimental value are shown in Fig. 12.

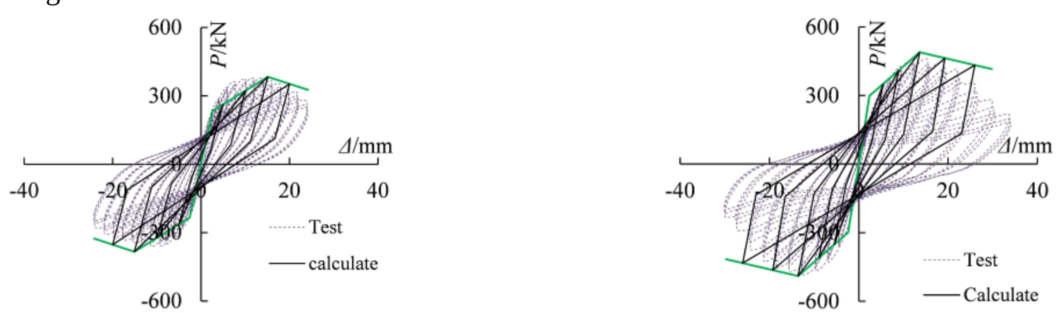

(a) SC1　　　　(b) SC12

Fig. 12—Comparison in hysteresis loop of calculated value and experimental value

6. Conclusions

In this paper the seismic behavior of sixteen specimens of concrete filled double steel plate (CFDSP) composite walls with binding bars were experimentally and numerical studied under axial compressive forces and reversed cyclic lateral loads. The proposed CFDSP wall exhibited good seismic behavior in the tests and could provide a favorable choice for the specific structural demand. The main conclusions drawn in this research can be summarized as follows:

(1) The CFDSP walls with binding bars exhibit excellent performance in shearing capacity, ductility, energy dissipation, lateral stiffness. It is a kind of composite elements of steel and concrete with outstanding seismic behavior.

(2) The configuration of CFDSP walls with binding bars is feasible. The bolt connection can effectively restrict the elements and improved the ductility. Embedment of channel steel can improve the shearing capacity of specimen.

(3) The factors of aspect ratios, axial compression ratios and binding bar spacing dramatically affected the seismic performance of this kind of shear walls. With the increase of the aspect ratios of the composite concrete and steel plate shear walls, the shearing capacity decreased obviously. The change of axial compression ratio has a certain effect on the horizontal shearing capacity of composite shear walls, but the influence is limited. The decrease of binding bars spacing can improve the shearing capacity.

(4) The calculated value by using the formula to computing lateral shearing capacity and deformation, the hysteretic model coincides well with the experimental value. The previous systematic studies laid a good foundation for engineering application. Some valuable results can give reference to the design and research of the new style shear walls.

7. Acknowledgements

This research is financial supported by the National Science Foundation of China (Grant No: 51178333). The author would also acknowledge the efforts and contributions from workers in the State Key Laboratory for Disaster Reduction in Civil Engineering at Tongji University.

8. References

1. Wright HD, Gallocher SC (1995). The behavior of composite walling under construction and service loading. J Constr Steel Res. **35:3**, 57–273.
2. Wright HD, Hossain K (1997). In-plane shear behavior of profiled steel sheeting. Thin Walled Struct .**29:1–4**, 79–100.
3. Wright H (1998). The axial load behavior of composite walling. J Constr Steel Res. 45(3):353–375.
4. Hossain K, Wright HD (1998). Performance of profiled concrete shear panels. J Struct Eng ASCE.**124:4**, 368-381.
5. Hossain K, Wright HD (2004). Experimental and theoretical behavior of composite walling under in-plane shear. J Constr Steel Res.**60:1**, 59–83.
6. Hossain K, Wright HD (2004). Performance of double skin-profiled composite shear walls —experiments and design equations. Can J Civ Eng .**31:2**, 204–217.
7. Emori K (2002). Compressive and shear strength of concrete filled steel box wall. Steel Structures.**68:2**, 29~40.
8. Bowerman HG, Gough MS, King CM (1999). Bi-Steel design and construction guide. British Steel Ltd..
9. Clubley SK, Moy S, Xiao RY (2003). Shear strength of steel–concrete–steel composite panels. Part I—testing and numerical modelling. J Constr Steel Res.**59:6**, 781–794.
10. Clubley SK, Moy S, Xiao RY (2003). Shear strength of steel–concrete–steel composite panels. Part II—detailed numerical modelling of performance. J Constr Steel Res .59(6):795–808.
11. Xie M, Chapman JC (2006). Developments in sandwich construction. J Constr Steel Res .**62:11SI**, 1123–1133.
12. JGJ 138-2001. Technical specification for steel reinforced concrete composite structures.